Journal of Computational and Applied Mechanics, Vol. 5., No. 2., (2004), pp. 209–222

NUMERICAL SIMULATION OF FLOW PAST A CYLINDER IN ORBITAL MOTION

László Baranyi
Department of Fluid and Heat Engineering, University of Miskolc
H-3515 Miskolc-Egyetemváros, Hungary
arambl@uni-miskolc.hu

[Received: January 19, 2004]

Abstract. A finite difference solution is presented for 2D laminar unsteady flow around a circular cylinder in orbital motion placed in a uniform flow for $Re = 130$, 160, and 180. Four cases displaying full lock-in are presented. The variation of time-mean and root-mean-square (rms) values of lift and drag coefficients were investigated against the amplitude of vibration in transverse direction. Abrupt jumps were found in the time-mean and rms values of lift and rms values of drag. These jumps seem to be caused by a change in the vortex structure.

Mathematical Subject Classification: 76B47, 76D25, 76M20
Keywords: circular cylinder, lock-in, orbital motion, vortex shedding, unsteady flow

Nomenclature

a_0	[-]	cylinder acceleration, nondimensionalized by U^2/d
A	[-]	amplitude of oscillation, nondimensionalized by d
C_D	[-]	drag coefficient
C_L	[-]	lift coefficient
d	$[m]$	cylinder diameter
D	[-]	dilation
f	[-]	oscillation frequency, nondimensionalized by U/d
p	[-]	pressure, nondimensionalized by ρU^2
Re	[-]	Reynolds number, Ud/ν
t	[-]	time, nondimensionalized by d/U
U	$[m/s]$	free stream velocity, velocity scale
u, v	[-]	velocities in x, y directions, nondimensionalized by U
x, y	[-]	Cartesian coordinates, nondimensionalized by d
ν	$[m^2/s]$	kinematic viscosity
ρ	$[kg/m^3]$	fluid density

Subscripts	
L	lift
D	drag
rms	root-mean-square value
x, y	components in x and y directions

1. **Introduction**

Flow-induced vibration of structures is encountered in various fields of engineering such as civil engineering, power generation and transmission, ocean engineering and offshore industry, aero-space industry, wind engineering. These motions are often not limited to one direction, i.e. they oscillate in both transverse and in-line directions. Oscillation in two directions can result in an orbital motion of the body, in which it follows an elliptical path.

Oscillatory flow has been fairly widely researched (e.g. [1]-[4]), as have oscillating cylinders in uniform flow (e.g. [5]-[9]). Also in fluid at rest, an orbiting cylinder has been investigated numerically by Teschauer et al. [10], while Stansby and Rainey [11] investigated a cylinder which was orbiting and rotating. However, research on an orbiting cylinder in uniform flow seems to have been neglected.

Earlier the author carried out computational investigations on a cylinder in orbital motion in a uniform stream at $Re = 180$ [12]. The orbital path resulted from the superposition of in-line and transverse oscillations, with frequencies of 85% that of the vortex shedding frequency from a stationary cylinders at that Reynolds number. The non-dimensional amplitude of oscillation in the in-line direction A_x was kept constant, while that of the transverse oscillation A_y was varied. At about A_y equals one-third of A_x, sudden jumps were observed in the time-mean value of the lift coefficient and in the root-mean-square (rms) values of lift and drag coefficients.

These unexpected results led the author to investigate this phenomenon further. It was thought that the jumps may be related to three-dimensional instability, called Mode A instability, occurring at around $Re = 188.5$ for a stationary cylinder as proven theoretically by Barkley and Henderson [13] and Posdziech and Grundmann [14], and experimentally by Williamson [15], although Norberg's results showed a somewhat lower value [16]. In this study, lower Reynolds numbers were also investigated ($Re = 130, 160$).

2. **Governing equations**

The governing equations are the two components of the Navier-Stokes equations, the continuity equation and the pressure Poisson equation written in dimensionless form in the non-inertial system fixed to the orbiting cylinder. The Navier-Stokes equations can be written as

$$\frac{\partial u}{\partial t} + u\frac{\partial u}{\partial x} + v\frac{\partial u}{\partial y} = -\frac{\partial p}{\partial x} + \frac{1}{Re}\nabla^2 u - a_{0x} \,, \tag{2.1}$$

$$\frac{\partial v}{\partial t} + u\frac{\partial v}{\partial x} + v\frac{\partial v}{\partial y} = -\frac{\partial p}{\partial y} + \frac{1}{Re}\nabla^2 v - a_{0y} \,, \tag{2.2}$$

where ∇^2 is the 2D Laplacian operator, a_{0x} and a_{0y} are the x and y components of the cylinder acceleration. In these equations the body force is included in the pressure terms. The equation of continuity has the form

$$D = \frac{\partial u}{\partial x} + \frac{\partial v}{\partial y} = 0 \,, \tag{2.3}$$

where D is the dilation. Taking the divergence of the Navier-Stokes equations yields the Poisson equation for pressure

$$\nabla^2 p = 2\left[\frac{\partial u}{\partial x}\frac{\partial v}{\partial y} - \frac{\partial u}{\partial y}\frac{\partial v}{\partial x}\right] - \frac{\partial D}{\partial t} \,. \tag{2.4}$$

No-slip boundary condition (BC) is used on the cylinder surface for the velocity and a Neumann-type condition is used for pressure p. A potential flow distribution is assumed far from the cylinder. We do not go into further details here (see [7, 17]).

3. **Transformation of domain**

Boundary conditions can be imposed accurately by using boundary fitted coordinates. In this way interpolation, often leading to poor solutions, can be omitted. By using unique, single-valued functions $g(\xi), f(\eta)$, the physical domain (x, y, t) can be mapped into a computational domain (ξ, η, τ) (see Figure 1):

$$x(\xi, \eta) = R(\eta)\cos[g(\xi)] \,, \tag{3.1}$$

$$y(\xi, \eta) = -R(\eta)\sin[g(\xi)] \,, \tag{3.2}$$

$$t = \tau \,, \tag{3.3}$$

where the dimensionless radius is

$$R(\eta) = R_1 \exp[f(\eta)] \,. \tag{3.4}$$

In this study the following linear mapping functions are used:

$$g(\xi) = 2\pi\frac{\xi}{\xi_{\max}}; \quad f(\eta) = \frac{\eta}{\eta_{\max}}\log\left(\frac{R_2}{R_1}\right) \,, \tag{3.5}$$

where subscript max refers to maximum value, R_1 is the dimensionless radius of the cylinder, and R_2 is that of the outer boundary of the computational domain (see Figure 1). Using equations (3.1) to (3.5) cylindrical coordinates with logarithmically spaced radial cells are obtained on the physical plane, providing a fine grid scale near the cylinder wall and a coarse grid in the far field.

Using equations (3.1) to (3.5), the governing equations and BCs (not shown here) can also be transformed into the computational plane. The transformed equations are solved by using the finite difference method, see e.g. [7, 17].

4. **Computational results**

The motion of the center of the cylinder is specified as follows

$$x_0(t) = A_x \cos(2\pi f_x t); \qquad y_0(t) = A_y \sin(2\pi f_y t) \ , \tag{4.1}$$

where A_x, A_y and f_x, f_y are the dimensionless amplitudes and frequencies of oscillations in x and y directions, respectively. Here $f_x = f_y$ which for nonzero A_x, A_y amplitudes gives an ellipse, the orbital path of which will become a circle when the two amplitudes are equal to each other. If one of the amplitudes is zero, in-line or transverse oscillation is obtained. When both amplitudes are zero, the cylinder becomes stationary.

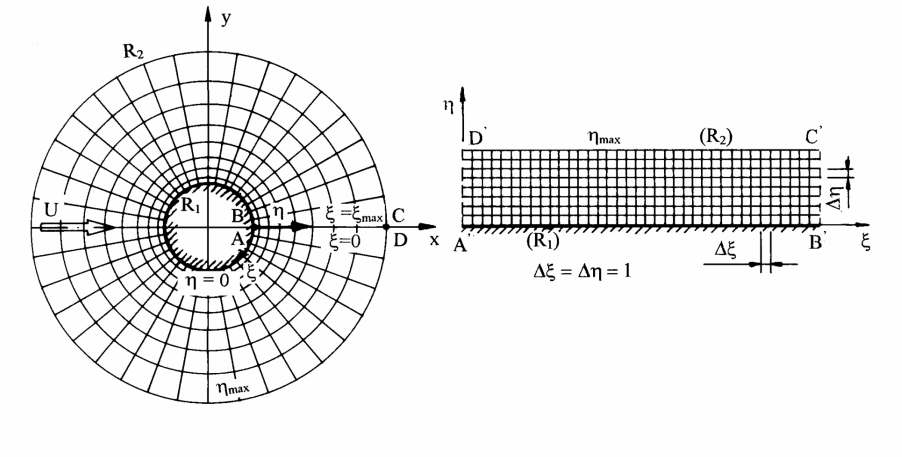

Figure 1. Physical and computational domains

Computations were carried out for Reynolds numbers 130, 160 and 180. The dimensionless frequencies f_x and f_y were kept constant at 85% of the frequency of vortex shedding from a stationary cylinder at that Reynolds number. This value was chosen because we wanted to reach lock-in without very large amplitudes of A_x and A_y.

Here, A_x was kept constant for a given Reynolds number while increasing the value of A_y. Various A_x values were used in computations; only those cases in which lock-in was reached at zero A_y value are shown in this paper. These were $Re = 130\,(A_x = 0.3)$, $Re = 160\,(A_x = 0.3)$, and $Re = 180\,(A_x = 0.3,\ A_x = 0.26)$. Lock-in is a phenomenon typical of oscillating structures. When the body is vibrating, either in forced or natural motion, a nonlinear interaction occurs as the frequency of the vibration approaches that of the vortex shedding. In this case vortex shedding occurs at the vibration frequency of the body, a phenomenon called lock-in.

In an earlier paper [12] computational results were shown for a cylinder in orbital motion at $Re = 180$ and $A_x = 0.3$. C_{Lrms}, C_{Drms} and $\bar{C}_D$, (the overbar denotes

time-mean value of the quantity) were shown against different A_y values. In that paper the time-mean and *rms* values were approximated based on the maximum and minimum values of the lift and drag coefficients. In the current study a more refined approach was applied to take into account the non-sinusoidal nature of the functions by following the integral definition of mean and *rms* values of a function f

$$\bar{f} = \frac{1}{nT} \int_{t_1}^{t_1+nT} f(t)\, \mathrm{d}t\,, \tag{4.2}$$

$$f_{rms} = \sqrt{\frac{1}{nT} \int_{t_1}^{t_1+nT} \left[f(t) - \bar{f}\right]^2 \mathrm{d}t}\,, \tag{4.3}$$

where t_1 is the starting time value for integration, T is the length of one cycle and n is the number of cycles. The *rms* and time-mean values were evaluated for a few n values in order to find the most precise fit. The original approach showed a sudden jump at $A_y = 0.1$ in all three values shown (C_{Drms}, C_{Lrms}, $\bar{C}_D$). The more precise current approach showed that, although the *rms* values are essentially the same, there is now only a small shift in $\bar{C}_D$ at $A_y = 0.1$. This indicates that signals should not be assumed to be sinusoidal in case of oscillating cylinders or those in orbital motion. While for a stationary cylinder, the simple original approach worked very well (showing that those signals are extremely near to sinusoidal shape), for oscillating cylinders Equations (4.2) and (4.3) should be used for evaluating time-mean and *rms* values.

Actually, C_L signals are rather distinctly asymmetric. Figures 2 and 3 show the time history of the lift coefficient at $Re = 160, A_x = 0.3$. In Figure 2, A_y is at 0.068 and the upper peaks are quite rounded and somewhat asymmetric, while the lower peaks are relatively sharp and more symmetric. In Figure 3, where A_y is just a little higher at 0.07, the pattern has reversed itself, with sharper upper peaks and more rounded lower peaks. In addition, the minimum value of C_L dropped substantially. The calculated mean value of the lift coefficient at $A_y = 0.068$ is 0.2432, and at $A_y = 0.07$ it is -0.3685 as seen in Table 2 in the Appendix. This rather drastic change is not limited to the lift coefficient.

Figures 4 to 6 (and their corresponding Tables, given in the Appendix) show the variations of time-mean and *rms* values of lift and drag coefficients C_L and C_D at $A_x = 0.3$ against A_y. As mentioned earlier, the frequency of oscillation in x and y directions (resulting in an elliptical path) was taken to be 85% of the vortex shedding frequency of a stationary cylinder at the same Reynolds number.

In Figure 4 (and Table 1), where $Re = 130$ and $f_x = f_y = 0.1521$, two sudden jumps were found in $\bar{C}_L$. Other values are just slightly affected at these critical A_y values. The time-mean value of $\bar{C}_D$ has practically no jump, and it slightly increases with increasing A_y values. Although it seems that $\bar{C}_D$ is hardly affected by the phenomenon that causes jumps in $\bar{C}_L$ values, C_{Drms} is influenced at the second critical point, though to a much lesser extent than $\bar{C}_L$. While passing through the

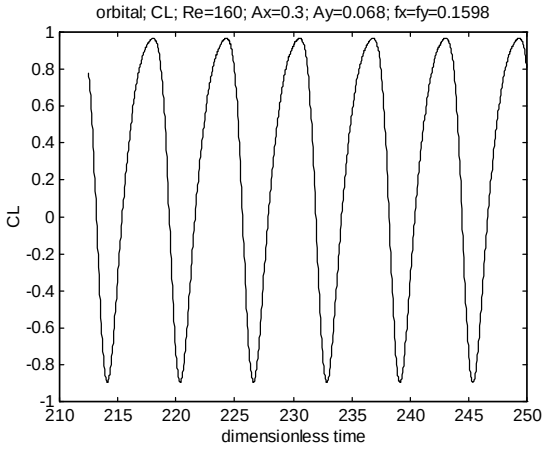

Figure 2. Time history of the lift coefficient for flow around a cylinder in orbital motion at $Re = 160$, $A_x = 0.3$, $A_y = 0.068$

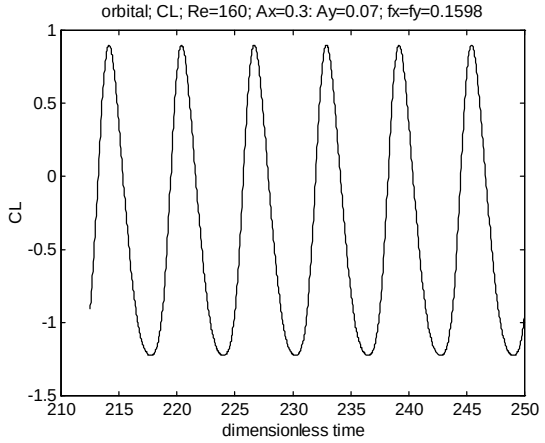

Figure 3. Time history of the lift coefficient for flow around a cylinder in orbital motion at $Re = 160$, $A_x = 0.3$, $A_y = 0.07$

critical values in A_y, there are also sudden changes in the shape of the time history curve of C_L, similar to those shown in Figures 2 and 3.

Time history signals for C_D also exhibited a change in amplitude after passing through the critical A_y values, although their shape was quite similar before and after. Before, between and after the jumps the slope of $\bar{C}_L$ is roughly identical and $\bar{C}_L$ decreases with increasing A_y approaching zero when A_y tends to A_x. After the second jump C_{Lrms} decreases and C_{Drms} increases with A_y.

In Figure 5 (and Table 2), where $Re = 160$ and $f_x = f_y = 0.1598$, only one sudden jump was found in $\bar{C}_L$. Here $\bar{C}_D$ seems to be insensitive to the phenomenon causing the jump in $\bar{C}_L$. The change in the shape of the C_L signal before and after the critical value A_y can be seen in Figures 2 and 3. Again, before and after the jump the slope of $\bar{C}_L$ is roughly identical. The *rms* values tend in opposite directions with A_y from those in Figure 4.

In Figure 6 (and Table 3), where $Re = 180$ and $f_x = f_y = 0.165665$, there are three sudden jumps in $\bar{C}_L$. Here $\bar{C}_D$ seems to be almost completely unaffected by the phenomenon that causes the jumps in $\bar{C}_L$. The change in the shape of the C_L signal while passing through the three critical A_y values is very similar to the changes shown in Figures 2 and 3. The slope of $\bar{C}_L$ between and after the jumps is again roughly identical. The variation of the *rms* values with A_y is very similar to that shown in Figure 5. Here $\bar{C}_L$ tends to about -0.5 as A_y tends to A_x. The *rms* curves are very similar to those shown in Figure 4.

Figure 7 (and Table 4) show the variations of time-mean and *rms* values of lift and drag coefficients at $A_x = 0.26$ against A_y for $Re = 180$. Just a small change (compared to Figure 6) in A_x resulted in a drastic change in the variation of $\bar{C}_L$ with A_y, while the other signals shown in Figures 6 and 7 are very similar to each other. All four variables are very similar to those in Figures 5 and 7.

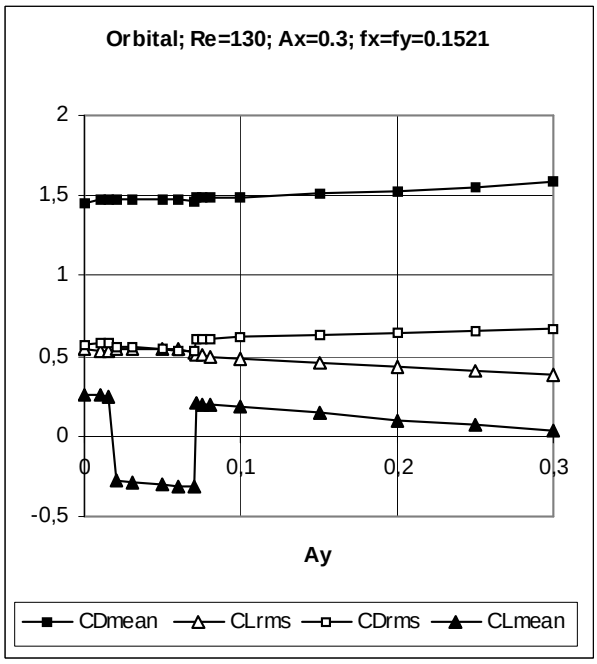

Figure 4. Time-mean and *rms* values of lift and drag coefficients versus A_y for $Re = 130$ and $A_x = 0.3$

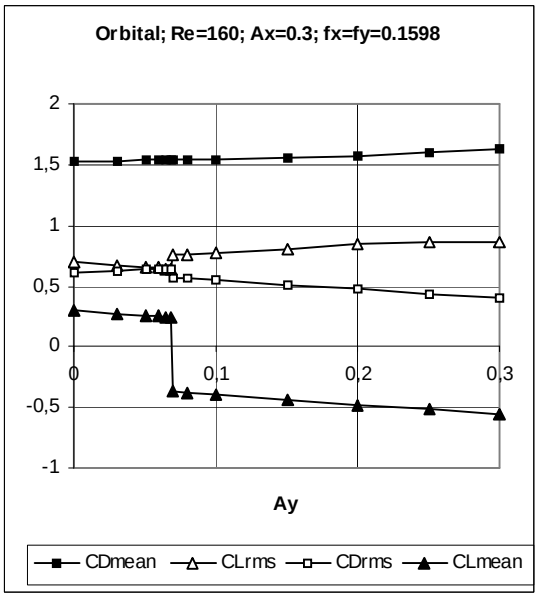

Figure 5. Time-mean and rms values of lift and drag coefficients versus A_y for $Re = 160$ and $A_x = 0.3$

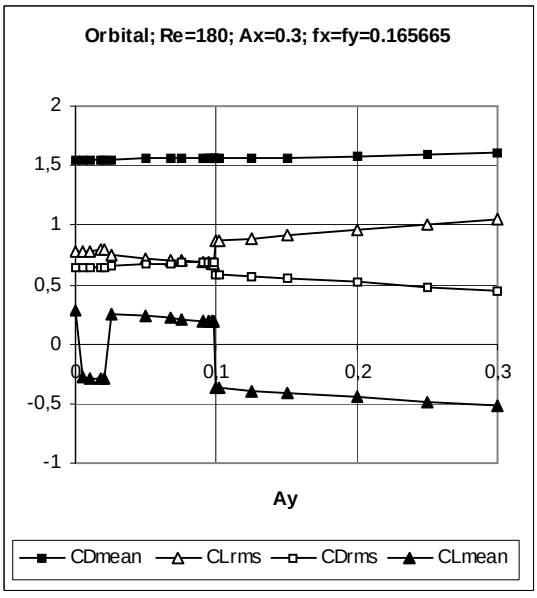

Figure 6. Time-mean and rms values of lift and drag coefficients versus A_y for $Re = 180$ and $A_x = 0.3$

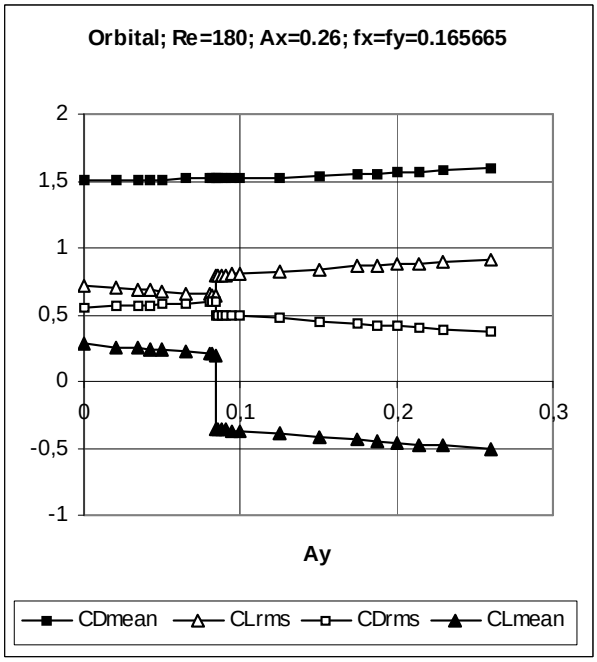

Figure 7. Time-mean and *rms* values of lift and drag coefficients versus A_y for $Re = 180$ and $A_x = 0.26$

To sum up, four cases were reported here. Reynolds numbers and the dimensionless amplitude of oscillation in the in-line direction A_x were kept fixed and the dimensionless amplitude of oscillation in transverse direction A_y was varied. One, two or three sudden jumps can be observed in the time-mean values of the lift coefficient $\bar{C}_L$ in each of the cases shown in Figures 4 to 7. The shape of the C_L signal changes abruptly while passing through the critical values of A_y values where the jumps take place. Interestingly, the slope of curve $\bar{C}_L$ is roughly identical before and after the jump(s). For all cases $\bar{C}_D$ seems to be almost completely unaffected by the phenomenon causing the jumps in $\bar{C}_L$ and it increases slightly with A_y. The *rms* values of the lift and drag coefficients have their most discernable jumps only at the highest critical A_y values. In case of $Re = 180$, these upper critical A_y values are practically equal to one third of A_x. This is not true for $Re = 130$ and 160. Somewhat unexpectedly, the direction in which *rms* values jump at the last critical A_y value differed: for $Re = 130$, where C_{Drms} jumped upwards and increased thereafter and C_{Lrms} jumped downwards and decreased, and for the other three cases, in which the directions were reversed.

While not shown here, base pressure coefficients were also calculated for $Re = 130$ and 160, and their time-mean and *rms* values also exhibit the same number of jumps as $\bar{C}_L$ at the same A_y values.

Our original possible explanation was that the jump(s) might have been caused by the 3D instability that occurs at around $Re = 188.5$ for a stationary cylinder. However, here we found that these jumps occurred at lower Reynolds number ($Re =$ 130 and 160) as well, so the instability explanation seems unlikely, unless instability zones are very different for oscillating cylinders compared to stationary cylinders. Experimental evidence (see e.g. [18, 19]) for oscillating cylinders shows that lock-in increases the span-wise correlation of signals and the two-dimensionality of the flow compared to flow around stationary cylinders. In [19] the increase in the cross correlation coefficient for velocity is actually used to identify lock-in. Poncet [20] shows how the 3D wake behind a circular cylinder can be made 2D by using lock-in triggered by rotary oscillation of the cylinder. These results suggest that the jumps are probably not caused by 3D instabilities. The only explanation we can offer at present is that the structure of vortices changes while going through the critical A_y values, which is represented by the change in lift coefficient signals as shown in Figures 2 and 3. There is a possibility that bifurcation occurs at these critical values. This phenomenon needs further investigation.

5. **Summary**

Flow around a circular cylinder in orbital motion placed in an otherwise uniform flow was investigated numerically using the computational method developed by the author, based on a finite difference solution. Four cases are shown in the paper: (a) $Re = 130$, $A_x = 0.3$; (b) $Re = 160$, $A_x = 0.3$; (c) $Re = 180$, $A_x = 0.3$; (d) $Re = 180$, $A_x = 0.26$. Reynolds numbers and the dimensionless amplitude of oscillation in the in-line direction A_x were kept fixed and the dimensionless amplitude of oscillation in transverse direction A_y was varied. Lock-in was observed at all A_y values. One, two or three sudden jumps can be observed in the time-mean values of the lift coefficient $\bar{C}_L$ for (a)-(d). The shape of the C_L signal changes abruptly while going through the critical values of A_y where the jumps take place. The slope of curve $\bar{C}_L$ is roughly identical before and after the jump(s). For all cases $\bar{C}_D$ seems to be almost completely unaffected by the phenomenon that caused the jumps in $\bar{C}_L$, unlike C_{Drms}. The rms values of the lift and drag coefficients have their most discernible jumps exactly at the highest critical A_y value.

The jumps were originally thought to have been possibly caused by the 3D instability that occurs at around $Re = 188.5$ for a stationary cylinder. However, the fact that jumps occurred at lower Reynolds numbers make this explanation unlikely. Furthermore, other researchers have found that lock-in states for oscillating cylinders strengthen the 2D effects, when compared to flow around stationary cylinders. The only explanation we can offer at present is that the vortex structure must change while passing through the critical A_y values. Further plans include further investigation of the phenomenon of the jumps and trying to find a physical explanation, beginning with the possibility of bifurcation effects.

Acknowledgement. The support provided by the Hungarian Research Foundation (OTKA, Project No. T 042961) is gratefully acknowledged.

REFERENCES

1. Bearman, P.W., Downie, M.J., Graham, J.M.R. and Obasaju, E.D.: Forces on cylinders in viscous oscillatory flow at low Keulegan-Carpenter numbers. *Journal of Fluid Mechanics*, **154**, (1985), 337-356.
2. Sarpkaya, T.: Force on a circular cylinder in viscous oscillatory flow at low Keulegan-Carpenter numbers. *Journal of Fluid Mechanics*, **165**, (1986), 61-71.
3. Yan, B.: Oscillatory flow beneath a free surface. *Fluid Dynamics Research*, **22**, (1998), 1-23.
4. Hu, P., Wu, G.X. and Ma, Q.W.: Numerical simulation of nonlinear wave radiation by a moving vertical cylinder. *Ocean Engineering*, **29**, (2002), 1733-1750.
5. Okajima, A.: Numerical analysis of the flow around an oscillating cylinder. *Proceedings of the Sixth International Conference on Flow-Induced Vibration*, London, 1995, 159-166.
6. Mittal, S. and Kumar, V.: Finite element study of vortex-induced cross-flow and in-line oscillations of a circular cylinder at low Reynolds numbers. *International Journal for Numerical Methods in Fluids*, **31**, (1999), 1087-1120.
7. Baranyi, L. and Shirakashi, M.: Numerical solution for laminar unsteady flow about fixed and oscillating cylinders. *Computer Assisted Mechanics and Engineering Sciences*, **6**, (1999), 263-277.
8. Dennis, S.C.R., Nguyen, P. and Kocabiyik, S.: The flow induced by a rotationally oscillating and translating circular cylinder. *Journal of Fluid Mechanics*, **407**, (2000), 123-144.
9. Mahfouz, I. and Badr, H.M.: Flow structure in the wake of a rotationally oscillating cylinder. *Journal of Fluids Engineering*, **122**, (2000), 290-301.
10. Teschauer, I., Schäfer, M. and Kempf, A.: Numerical simulation of flow induced by a cylinder orbiting in a large vessel. *Journal of Fluids and Structures*, **16**, (2002), 435-451.
11. Stansby, P.K., and Rainey, R.C.T.: On the orbital response of a rotating cylinder in a current. *Journal of Fluid Mechanics*, **439**, (2001), 87-108.
12. Baranyi, L. and Lakatos, K.: Computation of viscous flow around a circular cylinder in orbital motion in a uniform flow, *Proceedings of MicroCAD 2000, International Computer Science Conference*, Miskolc, 2000, 7-12.
13. Barkley, D. and Henderson, R.D.: Three-dimensional Floquet stability analysis of the wake of a circular cylinder. *Journal of Fluid Mechanics*, **322**, (1996), 215-241.
14. Posdziech, O. and Grundmann, R.: Numerical simulation of the flow around an infinitely long circular cylinder in the transition regime. *Theoretical and Computational Fluid Dynamics*, **15**, (2001), 121-141.
15. Williamson, C.H.K.: Vortex dynamics in the cylinder wake. *Annual Review of Fluid Mechanics*, **28**, (1996), 477-539.
16. Norberg, C.: Flow around a circular cylinder: Aspect of fluctuating lift. *Journal of Fluids and Structures*, **15**, (2001), 459-469.
17. Baranyi, L.: Computation of unsteady momentum and heat transfer from a fixed circular cylinder in laminar flow. *Journal of Computational and Applied Mechanics*, **4**(1), (2003), 13-25.

18. Bearman, P.W. and Obasaju, E.D.: An experimental study of pressure fluctuations on fixed and oscillating square-section cylinders, *Journal of Fluid Mechanics*, **119**, (1982), 297-321.

19. Koide, M., Tomida, S., Takahashi, T., Baranyi, L. and Shirakashi, M.: Influence of cross-sectional configuration on the synchronization of Kármán vortex shedding with the cylinder oscillation. *JSME International Journal*, Series B, **45**(2), (2002), 249-258.

20. Poncet, P.: Vanishing of B mode in the wake behind a rotationally oscillating cylinder. *Physics of Fluids*, **14**(6), (2002), 2021-2023.

6. **APPENDIX**

Tables 1 to 4 are appended here, containing time-mean and *rms* values for lift and drag coefficients versus dimensionless amplitude of transverse oscillation for different Reynolds numbers. These Tables contain the data on which Figures 4 to 7 were based.

Table 1. Time-mean and *rms* values of lift and drag coefficients for $Re = 130$ and $A_x = 0.3$

A_y	$\bar{C}_D$	C_{Lrms}	C_{Drms}	$\bar{C}_L$
0	1.4571	0.5409	0.5715	0.2641
0.01	1.4752	0.5357	0.5763	0.2556
0.015	1.4757	0.5335	0.5789	0.2514
0.02	1.4736	0.5467	0.5598	−0.2805
0.03	1.4735	0.5489	0.5540	−0.2886
0.05	1.4730	0.5488	0.5414	−0.3035
0.06	1.4719	0.5439	0.5345	−0.3096
0.07	1.4666	0.5250	0.5265	−0.3109
0.072	1.4858	0.5042	0.6051	0.2043
0.075	1.4858	0.5017	0.6065	0.2012
0.08	1.4870	0.4988	0.6086	0.1970
0.1	1.4930	0.4878	0.6168	0.1806
0.15	1.5099	0.4586	0.6340	0.1409
0.2	1.5317	0.4315	0.6479	0.1028
0.25	1.5567	0.4072	0.6596	0.0662
0.3	1.5846	0.3875	0.6696	0.0307

Table 2. Time-mean and *rms* values of lift and drag coefficients for $Re = 160$ and $A_x = 0.3$

A_y	$\bar{C}_D$	C_{Lrms}	C_{Drms}	$\bar{C}_L$
0	1.5316	0.6979	0.6110	0.3053
0.03	1.5331	0.674	0.6266	0.2779
0.05	1.5353	0.6580	0.6364	0.2598
0.06	1.5367	0.6500	0.6409	0.2506
0.065	1.5375	0.6460	0.6432	0.2461
0.068	1.5380	0.6436	0.6445	0.2432
0.07	1.5367	0.7522	0.5693	−0.3685
0.08	1.5382	0.7599	0.5630	−0.3771
0.1	1.5421	0.7747	0.5496	−0.3947
0.15	1.5560	0.8098	0.5145	−0.4371
0.2	1.5746	0.8412	0.4772	−0.4779
0.25	1.5985	0.8649	0.4385	−0.5173
0.3	1.6306	0.8629	0.3994	−0.5585

Table 3. Time-mean and *rms* values of lift and drag coefficients for $Re = 180$ and $A_x = 0.3$

A_y	$\bar{C}_D$	C_{Lrms}	C_{Drms}	$\bar{C}_L$
0	1.5524	0.7719	0.6481	0.2766
0.005	1.5521	0.7770	0.6453	−0.2827
0.01	1.5519	0.7818	0.6425	−0.2874
0.0175	1.5520	0.7890	0.6384	−0.2945
0.021	1.5514	0.7918	0.6364	−0.2990
0.025	1.5551	0.7478	0.6606	0.2544
0.05	1.5590	0.7241	0.6720	0.2310
0.0675	1.5624	0.7075	0.6796	0.2142
0.075	1.5636	0.7006	0.6829	0.2066
0.09	1.5671	0.6867	0.6889	0.1925
0.095	1.5686	0.6818	0.6907	0.1872
0.0975	1.5696	0.6792	0.6913	0.1851
0.09875	1.5696	0.6792	0.6913	0.1851
0.1	1.5560	0.8674	0.5887	−0.3696
0.1025	1.5566	0.8694	0.5869	−0.3727
0.125	1.5600	0.8906	0.5718	−0.3913
0.15	1.5643	0.9139	0.5547	−0.4114
0.2	1.5769	0.9604	0.5185	−0.4494
0.25	1.5909	1.0067	0.4819	−0.4825
0.3	1.6076	1.0532	0.4455	−0.5115

Table 4. Time-mean and rms values of lift and drag coefficients for $Re = 180$ and $A_x = 0.26$

A_y	$\bar{C}_D$	C_{Lrms}	C_{Drms}	$\bar{C}_L$
0	1.5093	0.7208	0.5509	0.2788
0.02	1.5099	0.7024	0.5619	0.2606
0.035	1.5115	0.6891	0.5694	0.2468
0.042	1.5106	0.6816	0.5722	0.2397
0.05	1.5122	0.6748	0.5760	0.2323
0.065	1.5167	0.6630	0.5834	0.2188
0.08	1.5201	0.6499	0.5900	0.2046
0.082	1.5209	0.6481	0.5905	0.2033
0.084	1.5212	0.6464	0.5915	0.2009
0.0845	1.5165	0.7919	0.5000	−0.3574
0.085	1.5178	0.7917	0.4990	−0.3596
0.088	1.5176	0.7943	0.4974	−0.3614
0.09	1.5180	0.7962	0.4961	−0.3629
0.095	1.5191	0.8001	0.4927	−0.3675
0.1	1.5205	0.8042	0.4893	−0.3720
0.125	1.5281	0.8238	0.4716	−0.3946
0.15	1.5379	0.8420	0.4530	−0.4170
0.175	1.5479	0.8605	0.4345	−0.4378
0.188	1.5540	0.8695	0.4247	−0.4484
0.2	1.5602	0.8768	0.4152	−0.4587
0.215	1.5683	0.8857	0.4035	−0.4711
0.23	1.5772	0.8935	0.3917	−0.4835
0.26	1.5970	0.9054	0.3682	−0.5078